Experimental and Theoretical Correlation of Reinforcement Trends in Acrylonitrile Butadiene Styrene/Single-Walled Carbon Nanotubes Hybrid Composites

Ahmad Nawaz Khan,[1] Qaiser Waheed,[1] Rahim Jan,[1] Khurram Yaqoob,[1] Zulfiqar Ali,[2] Iftikhar Hussain Gul[1]

[1]*Department of Materials Engineering, School of Chemical and Materials Engineering, National University of Sciences and Technology, Islamabad H-12, Pakistan*

[2]*Department of Chemical Engineering, COMSATS Institute of Information Technology, Lahore, Pakistan*

The reinforcement tendency of acrylonitrile butadiene styrene/single-walled carbon nanotubes hybrid composites is investigated using universal tensile testing machine. SWCNT are exfoliated in the ABS matrix at all concentrations, however, selective localization of SWCNT occurred in the SAN phase rather than the PB phase of ABS. Although, glass transition temperature of ABS remained intact by the incorporation of SWCNTs, but mechanical properties are enhanced significantly. The increase in tensile strength and Young's modulus of ABS/SWCNT hybrid composites is up to 48% and 103%, respectively, at considerable loss of strain at break inferring the restriction in the movement of the ABS chains by anchoring them in the vicinity of SWCNT. Modified rule of mixture (MRoM) model is employed to predict the rate of increase in the Young's modulus (dY/dV_f) of ABS/SWCNT hybrid composites. The predicted trends are correlated well with the experimental values of dY/dV_f in the lower volume fraction of SWCNT in ABS demonstrating the effective load transfer from the polymer matrix to the nanotubes. POLYM. COMPOS., 39:E902–E908, 2018. © 2017 Society of Plastics Engineers

INTRODUCTION

Hybrid organic–inorganic composites have spawned the research field owing to the achievement in reinforcement efficacy at very low loading levels (<5 wt%). The characteristics of the fillers such as filler size, shape, loading levels, and its dispersion as well as filler-polymer interactions play the major role in influencing the overall physical and mechanical properties of the polymers. Composites with various shapes of fillers like one-dimensional (1D), two-dimensional (2D), or three-dimensional (3D) have been incorporated in to different types of polymer matrices to obtain their effect from thermal to thermomechanical or rheological properties [1–9]. Particularly, 2D filler like graphene or layered clays and 1D like carbon nanotubes were more prone to induce the mechanical improvement in the polymer matrices [10–20]. Among these geometric shapes, composites show the maximum enhancement in their properties up to certain level of loading depending on the aspect ratio of the filler i.e. higher the aspect ratio; lower will be the concentration to induce the maximum enhancement in the mechanical properties.

Carbon nanotubes possess extraordinary mechanical properties such as modulus ≈0.27 to 1.0 TPa and tensile strength ≈11 to 63 GPa [21]. Although CNT is considered to be rigid and strong 1D cylindrical tubes but their reinforcement efficiency depends on the preparation method of composites, type of polymer, and type of functional moieties present on the surface of CNT to interact with the polymer chains. Recently, Puch and Hopmann [22] reported 25% increase in the tensile modulus of PA6/CNT up to 3.5 vol% while the tensile strength did not change in this range. While, Chen et al. [23] mentioned 87% and 69% increase of tensile modulus and tensile strength, respectively, up to 2 wt% for PA6/CNT composites due to the functionalization of amine groups on to CNT facilitating the interaction among filler and polymer chains. Additionally, the composite preparation method such as melt or solution method may also cause the variance in the improvement of the properties [24–26].

Correspondence to: A. Nawaz Khan; e-mail: ahmad.nawaz@scme.nust.edu.pk

Contract grant sponsor: Higher Education Commission (HEC) Pakistan under NRPU R and D (to A.N.K.); contract grant number: 20-3052.
DOI 10.1002/pc.24321
Published online in Wiley Online Library (wileyonlinelibrary.com).

In this research work, the reinforcement effect of SWCNT in acrylonitrile butadiene styrene (ABS) matrix is investigated. ABS copolymer is widely used due to its unique combinatorial properties of three different polymer systems giving high toughness along with good chemical resistance [27, 28]. SWCNT were dispersed uniformly in the SAN phase instead of PB phase. The mechanical properties of ABS are enhanced enormously in the presence of SWCNT. The increase in the mechanical properties is high at lower concentrations than at high concentrations of the nanofiller and plausible mechanism of enhancing the properties is also discussed. Moreover, the rate of increase in the Young's modulus (dY/dV_f) is a clear indicator of reinforcement trend and therefore, modified rule of mixture (MRoM) model is employed to predict the rate of increase of Young's modulus. The experimental rate of increase in the degree of reinforcement is correlated well with theoretical prediction of MRoM in the lower volume fraction demonstrating the effective load transfer from the polymer matrix to the nanotubes.

EXPERIMENTAL

Materials

ABS granules (PA-747, MFI = 1.1 g/10 min) were commercially provided by Zhenjiang ChiMei Co. Ltd. China. Single walled carbon nanotubes (SWCNT) having inner diameter of 1.1 to 2.3 nm, and average length of $\leq$5.0 μm were purchased from Sigma Aldrich Co. The density of SWCNT was 2.2 g/cm^3. The percentage of SWCNT in ABS was kept as 0.05, 0.24, 0.5, and 1.2 vol%, respectively.

Sample Preparation

For well dispersion of SWCNT in to ABS, the solvent casting method was used. ABS and SWCNT were dried for 5 h at 60°C before mixing to minimize the moisture content. The weighed amount of ABS was dissolved in 1,2-dichloroethane (DCE) and predetermined amount of SWCNT was mixed in the ABS solution. The solution was stirred for 24 h and sonicated for 1 h. The solution was casted at room temperature in a glass petri dish and left overnight for evaporation of solvent. Then the samples were placed in a vacuum oven at 70°C for 5 h to remove any remaining traces of solvent. The casted films were of 120 μm thickness and the samples were cut from the casted films of ABS and its composites for further characterization.

Characterization Techniques

X-ray Diffraction. X-ray diffraction patterns were measured at room temperature using a Theta-Theta instrument by STOE-Germany with a Cu-Kα Radiations ($\lambda = 0.15418$ nm) with an operating voltage and current of 40 kV and 40 mA, respectively, which uses a scintillation counter. The scanning rate was 2°/min over the range $2\Theta = 5°$ to 40°.

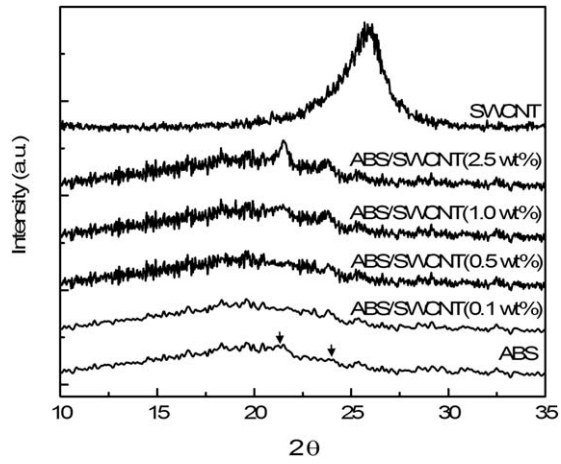

FIG. 1. X-ray diffraction patterns at different concentration of ABS/SWCNT hybrid composites.

Scanning Electron Microscopy (SEM). The morphologies of ABS and its nanocomposites were investigated using a JOEL JSM-6490A Analytical Scanning Electron Microscope. The samples were frozen by dipping in liquid Nitrogen and broken to generate the fresh surface. The samples were mounted on the Al stubs and coated with gold using a JOEL JFC-1500 Ion Sputtering device.

Differential Scanning Calorimetry. The thermal behavior was investigated using DSC (TA Q10) equipped with Liquid N_2. Dry N_2 gas was purged through DSC furnace at flow rate of 10 mL/min. The mass of the samples was kept ~5 mg and heating rate of 10°C/min was used. The temperature and heat flow rates were calibrated with indium and zinc standards.

Mechanical Properties. The tensile properties of ABS and its nanocomposite films were determined using Trapezium-X Universal Testing Machine (AG-20KNXD Plus) manufactured by Shimadzu Co. at a crosshead speed of 2 mm per minute (ASTM D882). The specimens used in these tests were prepared by cutting strips with dimensions of 80 × 10 × 0.12 mm^3 (length × width × thickness) with a gauge length of 20 mm (ASTM D6287). All the samples were tested at room temperature and at least five samples were used to obtain an average value.

RESULTS AND DISCUSSION

Structure and Morphology of ABS/SWCNT Hybrid Composites

Figure 1 shows the X-ray diffraction (XRD) patterns of ABS and its hybrid composites with single walled carbon nanotubes (SWCNT) at various concentrations. The graphitic peak of neat SWCNT appears at $2\Theta = 25.9°$

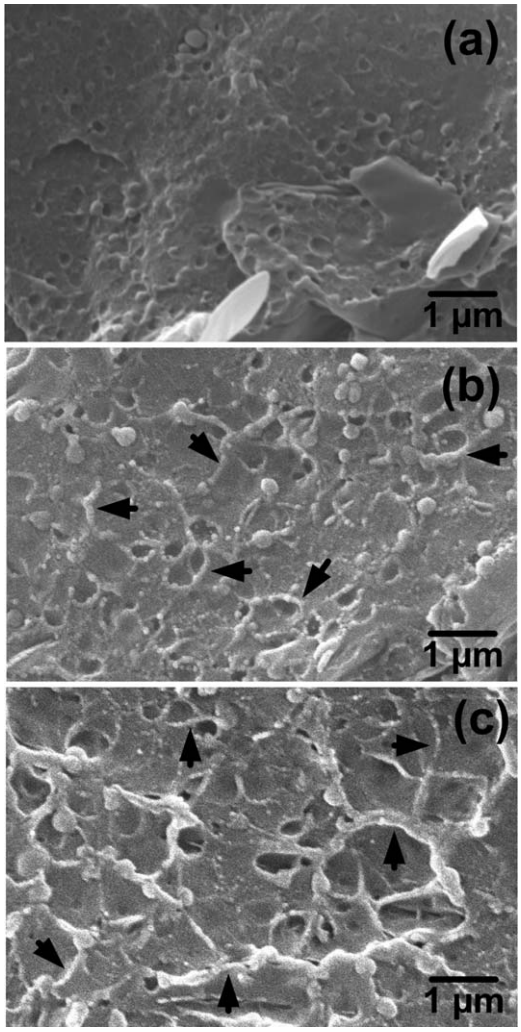

FIG. 2. SEM images of (a) neat ABS, (b) ABS/SWCNT at 0.24 vol%, and (c) ABS/SWCNT at 0.5 vol%.

whereas, the broad peak appears at $2\Theta = 20°$ for neat ABS indicating its amorphous structure. For hybrid composites of ABS/SWCNT, the disappearance of the graphitic peak clearly indicates the complete exfoliation of SWCNT in the ABS matrix for all the concentrations. Moreover, for ABS/SWCNT (1.2 vol%), small peak appears at $2\Theta = 21.5°$ and 23.8° inferring the ordering of the ABS chains in the presence of nanotubes. Notably, slight intensity of the peak for neat ABS is indicated by the arrows inferring the presence of localized ordering of the chains. However, the peak intensity increases by increasing the amount of SWCNT in ABS. Possibly, the phenyl and/or the nitrile groups of SAN phase in ABS arranges along the nanotubes due to their polar nature, eventually opting certain ordering of the chains to give some extent of crystallization in the ABS/SWCNT hybrid composites.

Figure 2 shows the SEM morphology for the dispersion of SWCNT in ABS matrix. In neat ABS, the sea-islands type of morphology is discernable in which polybutadiene (PB) islands in the form of nearly circular region are appearing in the sea of continuous SAN phase (Fig. 2a). The incorporation of SWCNT in ABS is dispersed randomly and uniformly throughout the matrix (Fig. 2b and c). However, the nanotubes are residing in the SAN phase as well as surrounding the PB phase as marked by arrows inferring the selective localization of nanotubes. Recently, M. H. Al-Saleh et al. [29] reported the dispersion of MWCNT in the SAN phase instead of PB phase of the ABS matrix. Moreover, Gao et al. [30] mentioned that in ABS, strong π-π interactions exists between the graphitic structure of graphene and the phenyl rings of SAN chains due to which the graphene layers were located in the SAN phase rather than in the PB phase. Therefore, SWCNT preferably reside in the SAN phase due to the non-covalent interactions among the graphitic structure of nanotubes and phenyl groups of SAN in ABS.

Thermal Behavior of ABS/SWCNT Hybrid Composites

The DSC graphs of ABS/SWCNT hybrid composites at various concentrations are shown in Figure 3. The value of glass transition temperature (T_g) for all the samples is determined from the midpoints of the downward step of the graphs. The T_g of neat ABS is 104.5°C and by the incorporation of SWCNT up to 0.24 vol%, the T_g is enhanced to 109.4°C indicating the constraining of chain mobility owing to the well dispersion of SWCNT at lower concentrations. Whereas, with further increase of SWCNT, T_g of ABS is decreased to 105°C, possibly due to the agglomeration at relatively higher concentrations. Usually, the decrease or increase as well as no change in the T_g of various polymer nanocomposites are reported [31–34]. For instance, Mari and Schaller [35] reported no difference in the T_g of ABS/CNTs composites at different concentrations determined by DSC. However, Yang et al. [36] investigated ABS/SWCNT composites and mentioned slight increase up to 6°C in the T_g value of ABS with increasing concentration of SWCNT to 10 wt%.

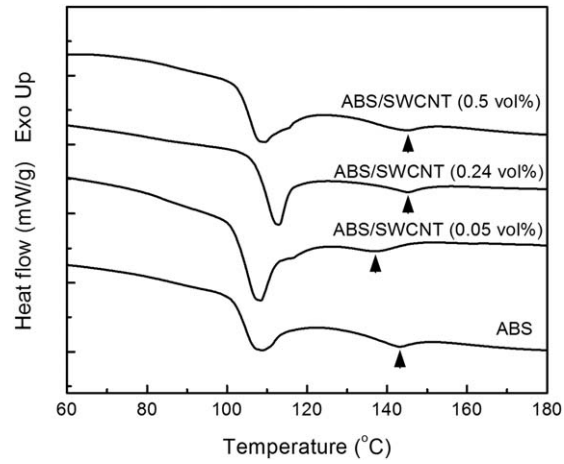

FIG. 3. DSC thermograms at different concentrations of ABS/SWCNT hybrid composites.

DOI 10.1002/pc

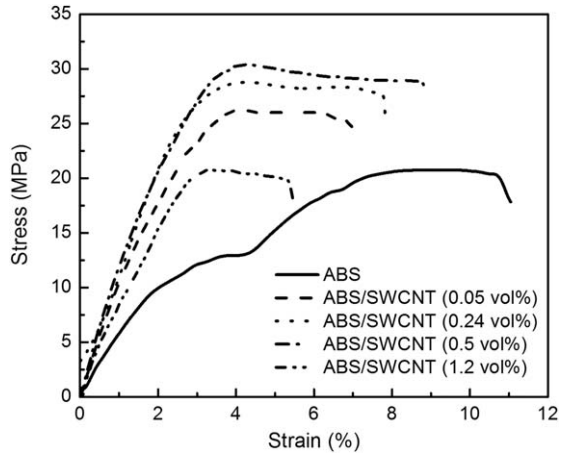

FIG. 4. The stress versus strain curves at various concentrations of ABS/SWCNT hybrid composites.

Additionally, there is an appearance of small endothermic peak around 143°C for ABS as well as ABS/SWCNT hybrid composites demonstrating the melting of the crystallites formed during the solidification of the samples. Clearly, DSC results are consistent with the X-ray results (Fig. 1) showing certain extent of crystallization in ABS/SWCNT composites. Sing et al. [37] also found similar results for ABS/MWCNT, having small endothermic peak around 140°C pertaining to the melting of the crystallites although no change in the T_g value of ABS occurred by the incorporation of 1.0 wt% of MWCNTs. Moreover, Jang et al. [38] reported ABS/nanoclay composites in which stretching of the phenyl and/or nitrile groups of SAN phase along the nanoclay layers was observed by FTIR spectra. Thereby, conjecturing that due to the polar nature of the phenyl and/or nitrile groups and their noncovalent interactions among ABS and the graphitic structure of the carbon nanotubes, the chains are arranged to give some extent of crystallization.

In our composite system, despite the well dispersion of the SWCNT in ABS matrix, although T_g remained unchanged but its influence on the mechanical properties of the ABS might vary which is further investigated and discussed.

Mechanical Properties of Hybrid Composites

Figure 4 shows the stress–strain graphs of ABS/SWCNT composites at different concentrations. Overall, the tensile properties of ABS are enhanced by the incorporation of SWCNT. The tensile strength of ABS/SWCNT composites (Fig. 5a) is concentration dependent. The maximum tensile strength of ABS is obtained up till 1.0 wt% of SWCNT, increasing up to 48% from 20.5 to 30.4 MPa. At higher concentration of SWCNT up to 2.5 wt%, the tensile strength of ABS hybrid composites is reduced to 20.7 MPa due to the possibility of agglomeration of the nanotubes in the matrix. Moreover, the strain at break of the ABS matrix is reduced with the addition of SWCNT (Fig. 5b). The maximum reduction of strain at break is up to 50% from 10.7 to 5.4% at 2.5 wt% of SWCNT in ABS matrix, attributing to the restriction in the movement of the polymer chains by anchoring them in the vicinity of SWCNT.

Furthermore, up to 1.0 wt% concentration of ABS/SWCNT hybrid composites, the Young's modulus is enhanced by about 103% from 511 to 1038 MPa (Fig. 6). Whereas increasing the SWCNT up to 2.5 wt%, the tensile modulus is decreased to 708 MPa, owing to the agglomeration of the nanotubes at higher concentrations. Recently, Heo et al. [39] reported the tensile properties of ABS/C18-graphene in which tensile modulus was increased by about 20% with the addition of 1.0 wt% nanofiller. While by increasing the concentration up to 3.0 wt% of C18-graphene, the tensile modulus was reduced. However, Al-Saleh et al. [40] mentioned the increase of tensile modulus up to 107% by the addition of 10 wt% of MWCNT in ABS matrix pertaining to the well dispersion and interaction of MWCNTs in ABS matrix at such higher concentration. Notably, the increase of tensile modulus of ABS/MWCNTs at 10 wt% is in the similar range which we have achieved at 1.0 wt% of SWCNT concentration. It clearly demonstrates that controlling the dispersion and interaction of the carbon nanotubes in the

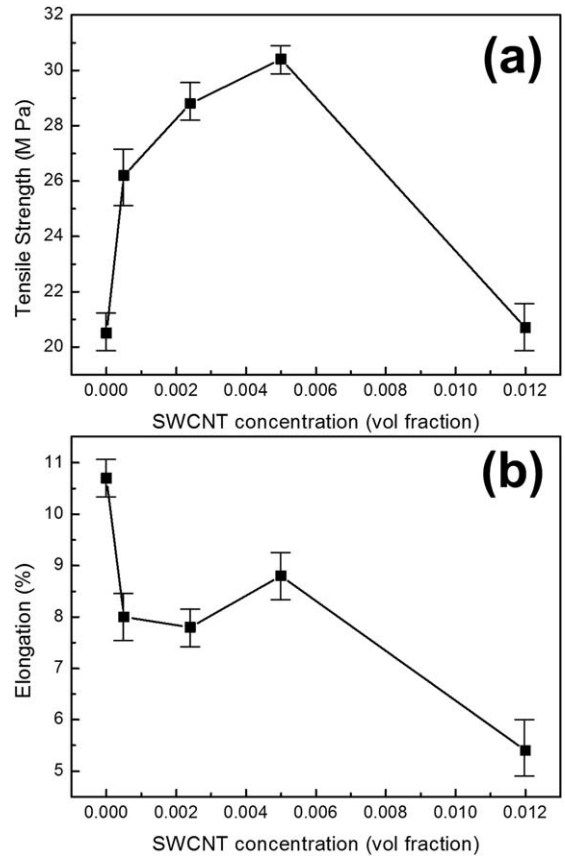

FIG. 5. The values of ABS/SWCNT obtained from the stress–strain curves for (a) tensile strength and (b) elongation at break.

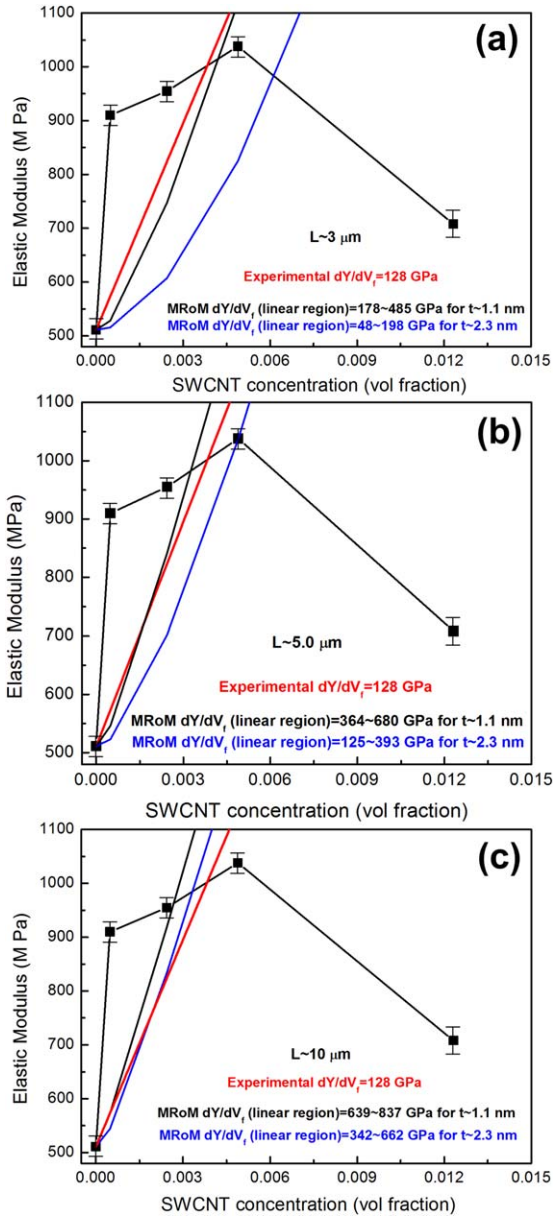

FIG. 6. The values of tensile modulus obtained from the stress–strain curves at various concentrations of ABS/SWCNT hybrid composites. The solid red line depicts the experimental rate of Young's modulus (dY/dV_f). MRoM model predicts the rate of increase of Young's modulus for differing the length of carbon nanotubes of (a) 3 μm, (b) 5 μm, and (c) 10 μm. The black and blue lines represent the theoretically calculated rate of increase in the Youngs modulus at 1.1 nm and 2.3 nm of nanotubes diameter, respectively.

ABS matrix, the enhancement in the mechanical properties can be achieved at much lower concentration. Additionally, the possibility of agglomeration or cluster formation of the carbon nanotubes would eventually reduce the mechanical properties of the polymer system.

The simplest possible theoretical explanation for reinforcement tendencies can be obtained on the basis of modified rule of mixtures (MRoM) given as under [41],

$$\mathrm{Yc(MRoM)} = (\eta\eta_0 Y_F - Y_M)V_f + Y_M \quad (1)$$

where Y_C, Y_F, Y_M, and V_f are Young's modulus of the composite, filler, polymer matrix and volume fraction of filler, respectively. In the above expression, η_0 is an orientation efficiency factor that is considered 0.2 for the random distribution of carbon nanotubes in the polymer matrix [42]. η is depicted as length efficiency factor. This term evaluates the matrix-fiber stress transfer effect, mainly dependent on the aspect ratio and Young's modulus of the filler along with the shear modulus of polymer matrix. The mathematical expression for length efficiency factor is presented as Ref. 43,

$$\eta(\mathrm{MRoM}) = 1 - \frac{\tan h(nL/d)}{nL/d} \quad (2)$$

where,

$$n = \sqrt{\frac{G_P V_f}{Y_f(1-V_f)}} \quad (3)$$

The term G_P represents the shear modulus of polymer matrix. Here in our case, the shear modulus of ABS is calculated to be 0.189 by using the following relationship, $Y_P = 2G_P(1+\nu)$ where υ is the Poisson ratio of ABS. Aspect ratio is given as L/d, where L is the length and d is the diameter of SWCNT.

To analyze the reinforcement effect of ABS/SWCNT hybrid composites on the basis of MRoM model, the experimentally found Young's modulus value of 511 MPa for ABS is used. The length of the SWCNT used in this work is varied ~3.0, 5.0, and 10 μm along with the diameter of 1.1 and 2.3 nm. The Young's modulus value range for SWCNT is ~1000 GPa [21, 44]. Figure 6 shows the experimental results for the Young's modulus of ABS/SWCNT hybrid composites. The Young's modulus values peak up as a function of SWCNT vol. fraction and maximum value of 1037 MPa is attained at 0.005 V_f. The rate of increase of Young's modulus (dY/dV_f) is a clear indicator of the reinforcement trend. Differentiating the *Eq. 1*, we get

$$\frac{dY}{dV_f}(\mathrm{MRoM}) \approx \eta\eta_0 Y_F - Y_M \quad (4)$$

The experimental dY/dV_f is around 128 GPa. The rate of reinforcement using MRoM model predicts the degree of reinforcement in the linear region. At $L = 3.0$ μm, dY/dV_f lies in the range of 48 to 178 GPa for $d = 1.1$ to 2.3 nm up to 0.005 V_f ABS/SWCNT composites. Increasing the $L = 5.0$ μm, dY/dV_f is raised to 125 to 364 GPa for $d = 1.1$ to 2.3 nm. By further increasing the $L = 10.0$μm, dY/dV_f is enhanced to 342 to 689 GPa for $d = 1.1$ to 2.3 nm. It clearly demonstrates that increasing the aspect ratio of SWCNT, the rate of increase in the degree of reinforcement would also enhance. In our case,

DOI 10.1002/pc

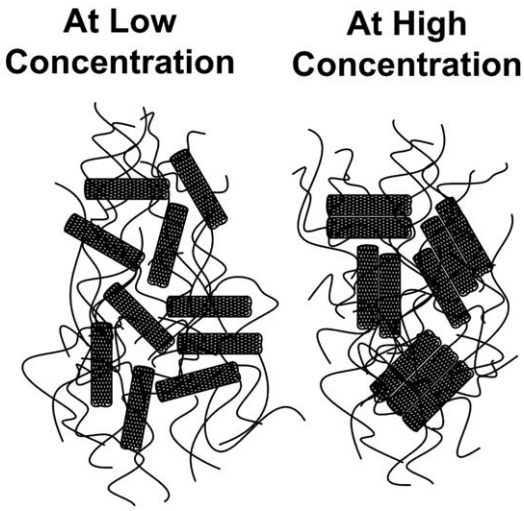

FIG. 7. Schematic representation of the dispersion of SWCNT in ABS at lower and higher concentrations.

considering the $L = 5.0$ μm with $d = 2.3$ nm matches more closely the predicted value of dY/dV_f with the experimental value of 128 GPa in the linear region up to 0.005 V_f of ABS/SWCNT hybrid composites.

Figure 7 shows the schematic for depicting the reinforcement effect at lower and higher concentrations of SWCNT in ABS. The factors contributing to the reinforcement efficiency are (i) well dispersion of the carbon nanotubes and (ii) good interfacial adhesion among carbon nanotubes and polymer matrix. As a result of well dispersion of the filler, the polymer chains can be anchored, giving rise to the reinforcement tendency [45]. While with good adhesion of the filler and matrix, the load can effectively be transferred from polymer matrix to the filler. Therefore, fulfilling both of these factors would overall enhance the tensile strength and modulus of the system in comparison with the neat polymer. In our system, SWCNT have noncovalent interactions with the ABS matrix, facilitating the adhesion of the ABS chains with the carbon nanotubes. Moreover, well dispersion is achieved at lower concentrations up to 1.0 wt%, resulting in the enhancement of the tensile strength and modulus. While, at higher concentrations, the nanotubes are stacked together owing to their van der Waals forces causing the agglomeration of the SWCNT. Thereby, the tensile strength and modulus of the system is reduced because agglomeration avoids the effective stress distribution and introduces the stress concentration centers for weakening the matrix.

CONCLUSIONS

The reinforcement effect induced by single walled carbon nanotubes (SWCNT) in acrylonitrile butadiene styrene (ABS) is investigated in this research work. The hybrid composites of ABS/SWCNT are prepared by solution casting method. In X-ray diffraction graphs, the absence of graphitic peak of SWCNT clearly infers the exfoliation of the nanotubes in the ABS matrix at all concentrations. SEM images show the selective localization of SWCNT in ABS in which nanotubes are preferably residing in the SAN phase rather than PB phase of ABS matrix possibly due to the non-covalent interactions among the graphitic structure of nanotubes and phenyl groups of SAN in ABS. Although, the glass transition temperature of ABS/SWCNT hybrid composites remained unchanged but the mechanical properties are enhanced significantly. The increase in tensile strength and Young's modulus of ABS/SWCNT hybrid composites was up to 48% and 103%, respectively. The rate of increase in the Young's modulus (dY/dV_f) is a clear indicator of reinforcement trend and modified rule of mixture (MRoM) is employed to correlate the experimental findings with the theoretical approach. At lower volume fraction of SWCNT in ABS, the experimental values of dY/dV_f matches well with the theoretical values obtained from MRoM model owing to better interaction and dispersion of the nanotubes in the ABS matrix.

REFERENCES

1. G. Mittal, V. Dhand, K.Y. Rhee, S.J. Park, and W.R. Lee, *J. Ind. Eng. Chem.*, **21**, 11 (2015).
2. X. Wang, Q. Jiang, W.Z. Xu, W. Cai, Y. Inoue, and Y.T. Zhu, *Carbon*, **53**, 145 (2013).
3. A.N. Khan, P.D. Hong, W.T. Cuang, and K.S. Shih, *Mater. Chem. Phys.*, **119**, 93 (2010).
4. H. Ma, L. Tong, Z. Xu, and Z. Fang, *Nanotechnology*, **18**, 375602 (2007).
5. A.N. Khan, A. Hayder, and W.T. Chuang, *Arab. J. Sci. Eng.*, **40**, 3373 (2015).
6. Y.S. Shim, and S.J. Park, *J. Nanosci. Nanotechnol.*, **12**, 5972 (2012).
7. A. Kasgoz, D. Akin, A.I. Ayten, and A. Durmus, *Compos. B*, **66**, 126 (2014).
8. Q. Waheed, A.N. Khan, and R. Jan, *Polymer*, **97**, 496 (2016).
9. K. Kanuga, and M. Cakmak, *Macromolecules*, **46**, 6300 (2013).
10. Y. Ma, D. Wu, Y. Liu, X. Li, H. Qiao, and Z.-Z. Yu, *Compos. B*, **56**, 384 (2014).
11. Y.C. Zhang, X.Y. Zhuang, J. Muthu, T. Mabrouki, M. Fontaine, Y. Gong, and T. Rabczuk, *Compos. B*, **63**, 27 (2014).
12. V.K. Tiwari, A.K. Prasad, V. Singh, K.K. Jana, M. Misra, C.D. Prasad, and P. Maiti, *Macromolecules*, **46**, 5595 (2013).
13. Z. Xu, and C. Gao, *Macromolecules*, **43**, 6716 (2010).
14. Y. Fu, L. Liu, J. Zhang, and W.C. Hiscox, *Polymer*, **55**, 6381 (2014).
15. K.M. Liew, Z.X. Lei, and L.W. Zhang, *Compos. Struct.*, **120**, 90 (2015).
16. A.N. Khan, M. Schmutz, J. Lacava, A.A. Ouahabi, T.T.T. Nguyen, P.J. Mesini, and J.M. Guenet, *Langmuir*, **31**, 7666 (2015).

17. A.N. Khan, and B.A. Ahmed, *Polym. Bull*., **72**, 1207 (2015).
18. S. Stankovich, D.A. Dikin, G.H.B. Dommett, K.M. Kohlhaas, E.J. Zimney, E.A. Stach, R.D. Piner, S.-B.T. Nguyen, and R.S. Ruoff, *Nature*, **442**, 282 (2006).
19. M. Cadek, J.N. Coleman, K.P. Ryan, V. Nicolosi, G. Bister, A. Fonseca, J.B. Nagy, K. Szostak, F. Beguin, and W.J. Blau, *Nano Lett*., **4**, 353 (2004).
20. J.N. Coleman, M. Cadek, R. Blake, V. Nicolosi, K.P. Ryan, C. Belton, A. Fonseca, J.B. Nagy, Y.K. Gun'ko, and W.J. Blau, *Adv. Funct. Mater*., **14**, 791 (2004).
21. M.F. Yu, O. Lourie, M.J. Dyer, K. Moloni, T.F. Kelly, and R.S. Ruoff, *Science*, **287**, 637 (2000).
22. F. Puch, and C. Hopmann, *Polymer*, **55**, 3015 (2014).
23. G.X. Chen, H.S. Kim, B.H. Park, and J.S. Yoon, *Polymer*, **47**, 4760 (2006).
24. U. Khan, K. Ryan, W.J. Blau, and J.N. Coleman, *Compos. Sci. Technol*., **67**, 3158 (2007).
25. R. Andrews, D. Jacques, M. Minot, and T. Rantell, *Macromol. Mater. Eng*., **287**, 395 (2002).
26. N. Mahmood, M. Islam, A. Hameed, S. Saeed, and A.N. Khan, *J. Compos. Mater*., **48**, 1197 (2014).
27. P. Svec, L. Rosik, R. Z. Horak, and F. Vecerka, *Styrene Based Plastics and Their Modifications*, Ellis Horwood, London, 145 (1990).
28. M. Chanda, and S. R. Roy, *Plastics Technology Handbook*, Marcel Dekker Inc., New York, 561 (1993).
29. M.H. Al-Saleh, H.K. Al-Anid, Y.A. Husain, H.M. El-Ghanem, and S.A. Jawad, *J. Phys. D: Appl. Phys*., **46**, 385305 (2013).
30. C. Gao, S. Zhang, F. Wang, B. Wen, C. Han, Y. Ding, and M. Yang, *ACS Appl. Mater. Interfaces*, **6**, 12252 (2014).
31. A.N. Khan, A. Hayder, W.T. Chaung, and P.D. Hong, *Polym. Sci. Ser. A*, **57**, 874 (2015).
32. S. Bandi, and D.A. Schiraldi, *Macromolecules*, **39**, 6537 (2006).
33. X. Zhang, and L.S. Loo, *Macromolecules*, **42**, 5196 (2009).
34. K.H. Liao, S. Aoyama, A.A. Abdala, and C. Macosko, *Macromolecules*, **47**, 8311 (2014).
35. D. Mari, and R. Schaller, *Mater. Sci. Eng. A*, **521**, 255 (2009).
36. S. Yang, J.R. Castilleja, E.V. Barrera, and K. Lozano, *Polym. Degrad. Stab*., **83**, 383 (2004).
37. B.K. Singh, P. Kar, N.K. Shrivastava, S. Banerjee, and B.B. Khutua, *J. Appl. Polym. Sci*., **124**, 3165 (2012).
38. L.W. Jang, C.M. Kang, and D.C. Lee, *J. Polym. Sci. Part B. Polym. Phys*., **39**, 719 (2001).
39. C. Heo, H.G. Moon, C.S. Yoon, and J.H. Chang, *J. Appl. Polym. Sci*., **124**, 4663 (2012).
40. M.H. Al-Saleh, B.A. Al-Saidi, and R.M. Al-Zoubi, *Polymer*, **89**, 12 (2016).
41. J. Rosenthal, *Polym. Compos*., **13**, 462 (1992).
42. R. Jan, P. May, A.P. Bell, A. Habib, U. Khan, and J.N. Coleman, *Nanoscale*, **6**, 4889 (2014).
43. G.E. Padawer, and N. Beecher, *Polym. Eng. Sci*., **10**, 185 (1970).
44. R.S. Ruoff, D. Qian, and W.K. Liu, *C. R. Phys*., **4**, 993 (2003).
45. R. Jan, A. Habib, M.A. Akram, T.H. Zia, and A.N. Khan, *Nanoscale Res. Lett*., **11**, 377 (2016).

DOI 10.1002/pc